

Surge of power transmission in flat and nearly flat band latticesH. Susanto,^{*} N. Lazarides[✉], and I. Kourakis[✉]*Department of Mathematics, Khalifa University of Science and Technology, P.O. Box 127788, Abu Dhabi, United Arab Emirates* (Received 13 February 2023; accepted 7 November 2023; published 22 November 2023)

Flat band systems can yield interesting phenomena, such as dispersion suppression of waves with frequency at the band. While linear transport vanishes, the corresponding nonlinear case is still an open question. Here, we study power transmission along nonlinear sawtooth lattices due to waves with the flat band frequency injected at one end. While there is no power transfer for small intensity, there is a threshold amplitude above which a surge of power transmission occurs, i.e., supratransmission, for defocusing nonlinearity. This is due to a nonlinear evanescent wave with the flat band frequency that becomes unstable. We show that dispersion suppression and supratransmission also exist even when the band is nearly flat.

DOI: [10.1103/PhysRevE.108.L052201](https://doi.org/10.1103/PhysRevE.108.L052201)

Introduction. Flat band lattices are periodic media with at least one of their Bloch bands completely flat in the entire Brillouin zone (see, e.g., [1–3] for early theoretical predictions). Because the wave group velocity vanishes, the media are dispersionless and, as such, wave transport is suppressed and particles will have infinite effective mass, which brings forth exotic characteristics and dynamics (see, e.g., the recent reviews [4–7]). As the kinetic energy is completely quenched, particle interaction becomes enhanced, which makes flat band lattices a perfect candidate to study complex many-body quantum states and strongly correlated physical systems [2,8,9]. Linear flat band lattices also support localized modes without inhomogeneity that have been demonstrated theoretically [10–14] and observed experimentally [15–18]. In interacting with nonlinearity, flat bands can support compactons [10] and interaction-driven topological states [19].

Here we are interested in the scattering of plane waves by a nonlinear medium which possesses a flat band. Due to the dispersionless property of the medium, what happens when the plane wave frequency falls within the flat band is a mystery. One may expect that the wave will be totally reflected, but it is not certain. Moreover, the presence of nonlinearity can alter expected behaviors and the dynamics can become complicated. An important example is the so-called supratransmission, i.e., an abrupt transmission phenomenon of plane wave power with frequency in the forbidden band when the incoming wave amplitude is above a threshold, that has been reported both theoretically and experimentally [20–25].

Here, we report a supratransmission of plane waves with *frequency in the flat and nearly flat band* when the wave amplitude is above a critical value. As a particular case, we consider the sawtooth lattice with Kerr nonlinearity, and to represent incoming plane waves the medium is periodically end driven.

The sawtooth lattice (portrayed in Fig. 1) belongs to a class of quasi-one-dimensional lattices with an accidental flat band, i.e., a flat band that is formed only when a special relation between its coupling coefficients holds [11,26]. The presence of an accidental flat band was observed on waveguides arranged on a sawtooth lattice by fine tuning the intersite coupling coefficients [27].

Sawtooth lattices have been investigated in many diverse physical contexts including photonics [28,29], Bose-Hubbard systems [30], the attractive Hubbard model [31], strongly interacting bosons [32], Bose-Einstein condensates [33], and ultracold atoms [34]. Because completely flat bands of the sawtooth lattice are sensitive to perturbations (e.g., of the coupling coefficients), in the following we consider the general case of nearly flat bands, where the characteristics of wave inhibition and supratransmission will be shown to be generic.

We also study the mechanism behind the surge of transmission phenomenon. In the standard case, it is caused by the generated sequence of gap solitons propagating in the medium. Supratransmission in lattices with a flat band was considered in [35], where generation of gap solitons with zero frequency drive was shown to be possible. However, similar nonlinear modes cannot exist within flat or nearly flat bands. The supratransmission reported herein is therefore different. In fact, we show that in the case of a completely flat band, the surge is due to the instability of a nonlinear edge state with the flat band frequency.

Model equation. The semi-infinite sawtooth lattice is modeled by

$$\begin{aligned} i\dot{A}_n &= C_A(\Delta_+ B_{n-1} - 2A_n) + \gamma |A_n|^2 A_n, \\ i\dot{B}_n &= C_A(\Delta_+ A_n - 2B_n) + C_B \Delta B_n + \gamma |B_n|^2 B_n, \end{aligned} \quad (1)$$

where the upper dot is the derivative with respect to the time variable t (or the propagation distance in nonlinear optics), $n \in \mathbb{Z}^+$, $\Delta_+ X_n = X_n + X_{n+1}$, $\Delta X_n = X_{n-1} + X_{n+1} - 2X_n$, and γ is the nonlinearity coefficient. The lattice is driven through its left boundary by setting $B_0 = f(t)$, with $f(t) = F(t)e^{-i\Omega t}$. The amplitude of this harmonic force is turned on

^{*}Corresponding author: hadi.susanto@ku.ac.ae

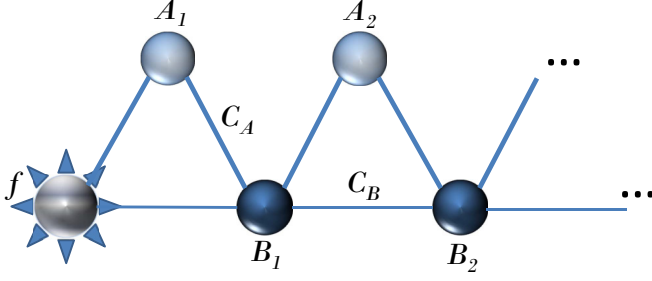


FIG. 1. Schematic representation of the semi-infinite one-dimensional lattice in the model, driven at the edge by f .

adiabatically, e.g., as $F(t) = f_0[1 - \exp(-t/\tau)]$, $\tau \gg 1$, to avoid initial shock.

The linear plane wave of the (infinite) lattice is given by $\{A, B\}_n = \{a, b\}e^{i(kn - \omega t)}$, where

$$\omega_{\pm} = C_B(\cos k - 1) - 2C_A \pm \sqrt{\tilde{\omega}}, \quad (2)$$

and $\tilde{\omega} = C_B^2(\cos k - 1)^2 + 2C_A^2(\cos k + 1)$, with the corresponding eigenvectors $(a, b) = (C_A(1 + e^{-ik}), \omega_{\pm} + 2C_A)$. This implies that the lattice has two linear bands at $-2C_A \leq \omega \leq 0$ and $-\max(v) \leq \omega \leq -\min(v)$, where $v = \{C_A + 2C_B, 4C_A\}$. The latter band becomes flat when $C_A = 2C_B$ [11,26]. We plot the bands in Fig. 2. Without loss of generality, we take $C_B = 1$.

When the driving frequency Ω of the external force lies within a linear band, there will be power flow through the lattice even for low amplitude driving [21,22]. However, note that the flow speed is given by the group velocity $\partial\omega/\partial k$. Because $\partial\omega/\partial k \rightarrow 0$ as $C_A \rightarrow 2C_B$, what happens when the driving frequency Ω is at the flat or in a nearly flat band? This is the main question that we consider in this Letter.

Supratransmission. Equations (1) were numerically integrated in time using a sixth order Runge-Kutta scheme [36] with time step $h = 5 \times 10^{-3}$. The semi-infinite lattice is truncated into a finite one with $N = 256$ unit cells, and dissipation is imposed by adding the terms $-i\Gamma_n A_n$ and $-i\Gamma_n B_n$ on the right-hand side of Eqs. (1), respectively, to suppress wave reflection from the right boundary of the lattice. The dissipation array Γ_n is zero for $n = 1, \dots, N - N_d$, and $\Gamma_n = \Gamma_{\max}(n -$

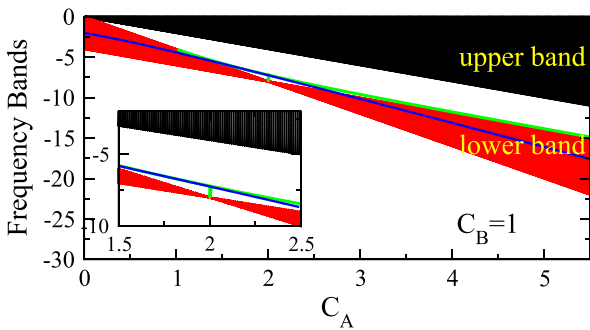


FIG. 2. Two allowed bands of the system as a function of the coupling coefficient C_A . Additionally, there is an in-gap eigenfrequency for *finite* lattices shown as a green curve (see the text). Analytical approximation $\tilde{\omega}_-$ (5) is shown in blue. Inset: Enlargement around $C_A = 2C_B = 2$.

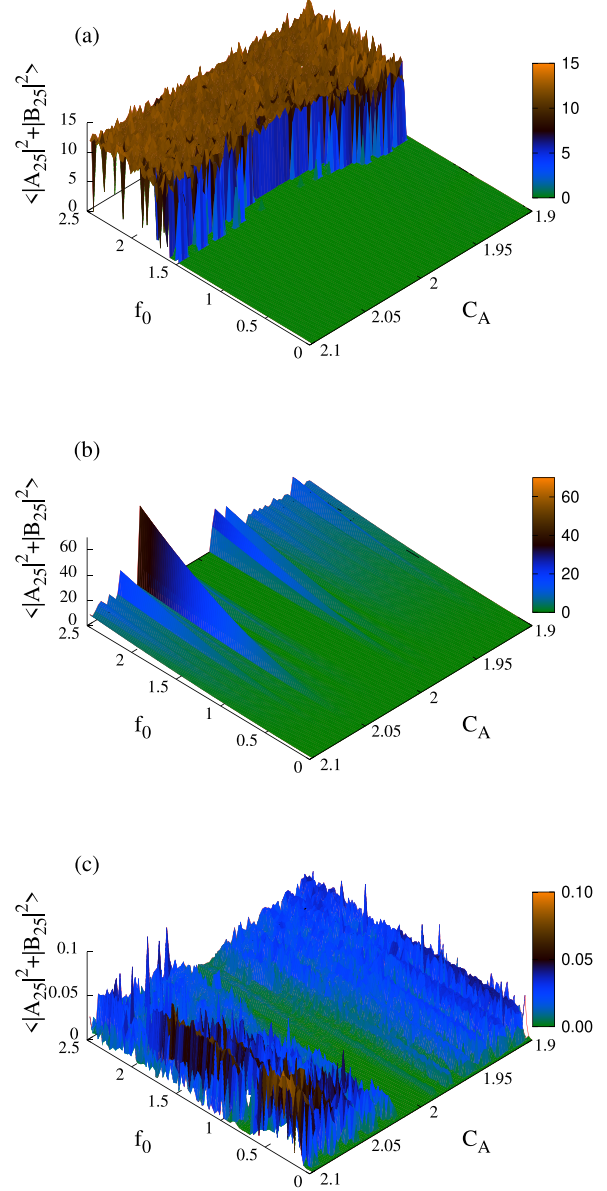


FIG. 3. The averaged power at the 25th cell, $\langle |A_{25}|^2 + |B_{25}|^2 \rangle$, as a function of the driving force amplitude f_0 and the coupling coefficient C_A for $C_B = 1$, and (a) $\gamma = -2$, (b) $\gamma = 0$, and (c) $\gamma = +2$.

$N + N_d)/N_d$ for $n = N - N_d + 1, \dots, N$ ($\Gamma_{\max} = 5$). Herein, $N_d = 32$.

Next, we study the flow of power injected by the drive into the array. To show our results, we compute the time-averaged power at a particular site $\langle |A_{25}|^2 + |B_{25}|^2 \rangle$, which is far enough from the driving edge. We integrate the governing equation and discard the first $T_{\text{tr}} = 200\,000 T$ time units, where $T = 2\pi/\Omega$ is the driving period. The integration continues for $T_{\text{av}} = 50\,000 T$ more time units, where the average power is then calculated. We present it in Fig. 3 as a function of the driving force amplitude f_0 and C_A for several values of γ . In all cases, the driving frequency is $\Omega = -(3C_A + 2C_B)$, i.e., in the middle of the lower band.

For the defocusing nonlinearity $\gamma = -2$ the power transmission to the cell at $n = 25$ is very low, until a C_A -dependent

threshold value of $f_0 = f_0^{\text{th}}$ is reached, where it jumps abruptly to high values of the order of 10. For $C_A = 2$, $f_0^{\text{th}} \approx 1.668$. Below the threshold, the value of the transmitted power is of the order of 10^{-5} or less. For $f_0 > f_0^{\text{th}}$, the transmission remains at high levels and nearly constant on average. For $\gamma = 0$ (linear regime), the transmission increases gradually and nonlinearly with increasing f_0 . However, different from the defocusing case above, the transmission power diminishes at the flat band only. As soon as the lower band is not completely flat, there is a significant power transmission. For the focusing nonlinearity $\gamma = +2$, a different situation is observed in Fig. 3(c), where the transmission is low in the whole parameter plane shown with the lowest transmission again around $C_A = 2$.

Thus, the main effect which differentiates these three regimes is the existence of the threshold f_{th} for defocusing nonlinearity which leads to a sharp transition from low to high power transmission at that amplitude.

Bifurcation of evanescent waves. Supratransmission has been previously shown to be caused by an evanescent wave that ceases to exist [22–24] in a turning point bifurcation. It is then instructive to consider the standing wave solution of (1) with frequency Ω . Substituting $\{A, B\}_n = \{a, b\}_n e^{-i\Omega t}$, we obtain the following coupled algebraic equations:

$$\begin{aligned} \Omega a_n &= C_A(\Delta_+ b_{n-1} - 2a_n) + \gamma a_n^3, \\ \Omega b_n &= C_A(\Delta_+ a_n - 2b_n) + C_B \Delta b_n + \gamma b_n^3, \end{aligned} \quad (3)$$

where $b_0 = f_0$.

We shall look for solutions of the system that are localized close to or at the driven end of the sawtooth lattice, while they decay to zero relative far from it. These evanescent modes owe their very existence to the localized eigenmodes associated with the flat band, which are expected to be stable for low f_0 (weak nonlinearity).

Once a solution is found, its linear stability is computed through solving the corresponding eigenvalue problem obtained from substituting $A_n = (a_n + \hat{a}_n e^{\lambda t}) e^{-i\Omega t}$ and $B_n = (b_n + \hat{b}_n e^{\lambda t}) e^{-i\Omega t}$ into the governing equations (1) and linearizing about small \hat{a}_n and \hat{b}_n . The solution is said to be linearly stable if all the spectrum λ has zero real part.

In Fig. 4(a) we present a bifurcation diagram of the nonlinear mode as a function of the driving amplitude f_0 in the defocusing case ($\gamma = -2$) for $C_A = 2$. Starting from the lower branch that corresponds to evanescent waves appearing as one ramps up the external drive $f(t)$, we obtain that the corresponding solution is stable. As we increase f_0 further, there is a critical value where the solution becomes unstable due to a quartet of complex eigenvalues. In the figure, this occurs at $f_0^{\text{cr}} \approx 1.730$, which is in close agreement with the threshold amplitude f_0^{th} reported above.

The small difference between f_0^{th} and f_0^{cr} is due to the strong instabilities which are present in the numerical integration of the dynamical equations (1) that produce irregular behavior especially when the threshold driving amplitude is approached.

Hence, we obtain that the supratransmission in Fig. 3(a) above corresponds to the evanescent wave becoming unstable. This mechanism is different from the previously reported cases [21–23], where the threshold amplitude occurs at a turning point.

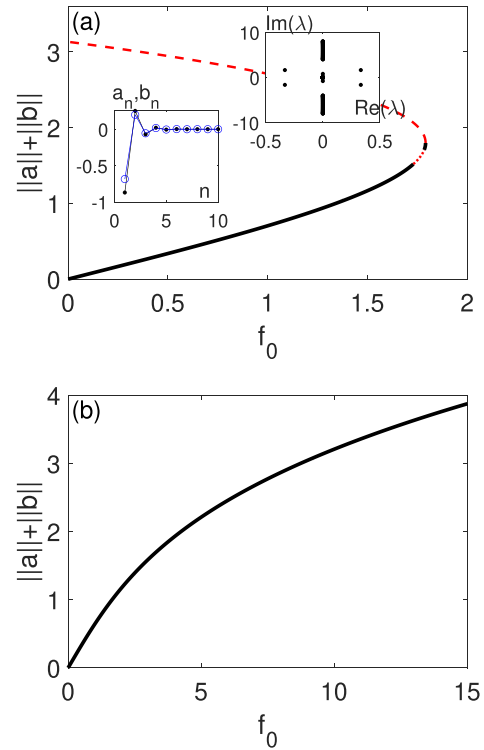


FIG. 4. Bifurcation diagram of localized solutions of (3) as a function of the driving amplitude f_0 for (a) $\gamma = -2$ and (b) $\gamma = +2$. Shown is the norm on the vertical axis, where $\|a\| = \sqrt{\sum_1^n |a_n|^2}$ and $\|b\| = \sqrt{\sum_1^n |b_n|^2}$. The inset shows the most unstable solution profile on the lower branch and the corresponding linear spectrum in the complex plane. Solid (dashed) lines represent stable (unstable) solutions.

After instability in the lower branch, as we increase f_0 further, we obtain a small portion where the decaying-in-space solution becomes stable again. The localized wave then ceases to exist due to a turning point bifurcation at $f_0^{\text{TP}} \approx 1.791$. The upper branch corresponds to solutions that are exponentially unstable due to a pair of real eigenvalues.

We have also calculated nonlinear evanescent waves due to the drive in the focusing case in Fig. 4(b), where there is no change of stability nor turning point. This explains the absence of supratransmission in the focusing case in Fig. 3(c).

When the lower band is nearly flat, i.e., $C_A \approx 2C_B$, our evanescent wave analysis above cannot be applied because there is no spatially decaying state in the middle of the band. Nevertheless, extreme suppression of power is clearly seen in Figs. 3(a) and 3(c) when the system is nonlinear. This peculiar phenomenon is caused by nonlinear interaction between the in-band drive and its in-gap excited harmonics. The supratransmission in the defocusing nonlinearity case is then caused by the corresponding evanescent modes of the resonant harmonics becoming unstable. This argument will be clearly seen from the time-series analysis below.

Time-series analysis. We have performed Fourier spectral analysis of the dynamics of the end-driven lattice. In Fig. 5, the decimal logarithms of Fourier spectra for $A_1(t)$, $\log_{10}[FT\{A_1\}]$, are shown for the complete flat band case $C_A = 2$ and several values of the driving amplitude f_0 . The

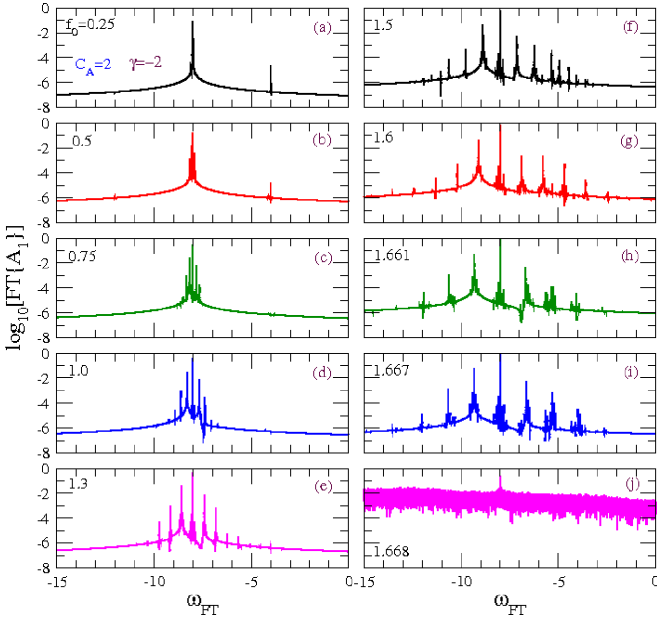


FIG. 5. Fourier spectra of $A_1(t)$ for several values of driving amplitudes f_0 for $C_B = 1$, $\gamma = -2$, and $C_A = 2$, shown in semilogarithmic plots.

time series are recorded after integrating the system for $10^5 T$ to eliminate transients. The length of each time series spans a time interval of more than $1.6 \times 10^4 T$; each time series consists of $N_{FT} = 2^{19}$ points. The resolution in the Fourier frequencies is therefore $\Delta\omega_{FT} \simeq 2.4 \times 10^{-4}$.

For low f_0 , much lower than the threshold value, the driving frequency is dominant. One may also observe a second (sub)harmonic in the spectra in Figs. 5(a) and 5(b). The frequency, which is at $\omega_{FT} \approx -4$, corresponds to the lower edge of the top band (see Fig. 2).

With increasing f_0 , however, it disappears due to increasing nonlinearity strength that results in gradual weakening of the resonance and its subsequent disappearance. At the same time, more subharmonics around the driving frequency appear.

Their separation increases with the increment of f_0 and is maintained at an equidistant space for values of f_0 even very close to the threshold. When f_0 exceeds the threshold, the spectrum changes drastically, as it can be observed in Fig. 5(j). This change occurs abruptly, indicating once more that the passage from very low to very high transmission is a real transition. After the transition, the Fourier spectrum becomes essentially continuous and rather noisy, while significant power is acquired by all the frequencies in the shown range. Even in this regime, the driving frequency is still visible and dominant.

The equidistant subharmonics appear because the external driving force excites and resonates with an internal edge mode of the semi-infinite system, which can be explained as follows.

Consider the linear parts of Eqs. (1), i.e., set $\gamma = 0$ with $f_0 = 0$, and substitute $A_n = \hat{a}_n e^{-i\omega t}$ and $B_n = \hat{b}_n e^{-i\omega t}$. We end up with an eigenvalue problem for the eigenfrequency ω and eigenmodes (\hat{a}_n, \hat{b}_n) , that has been solved numerically for the same finite number of unit cells. We plot ω in Fig. 2 and obtain

that in addition to the two continuous bands (2), there is an isolated spectrum shown in the green curve.

The eigenfrequency can be observed to get detached from the lower band at $C_A = 1$ and persist as an isolated in-gap eigenfrequency even for large C_A . This frequency is associated with a localized eigenmode having topological origin [27,30]. The inset in Fig. 2 shows it more clearly in a shorter C_A interval. Note that $C_A = 2C_B$ is a singular case as the in-gap eigenfrequency merges with the flat band.

The edge eigenmode is highly localized for the parameter value slightly above $C_A = 2$. This motivates us to consider the following unit cell at the driven edge:

$$\begin{aligned} i\dot{A}_1 &= C_A[f + B_1 - 2A_1] + \gamma|A_1|^2 A_1, \\ i\dot{B}_1 &= C_A(A_1 - 2B_1) + C_B[f - 2B_1] + \gamma|B_1|^2 B_1. \end{aligned} \quad (4)$$

We expect that this system is an approximation of the model (1) with an error of $\mathcal{O}(1/|\Omega|)$ for $|\Omega| \gg 1$ [23]. It is standard to obtain that in the linear limit $\gamma = 0$, the solution of Eqs. (4) involves three frequencies: Ω and

$$\hat{\omega}_{\pm} = -(2C_A + C_B) \pm \sqrt{C_A^2 + C_B^2}. \quad (5)$$

We plot $\hat{\omega}_-$ in Fig. 2, where good agreement is clearly seen in a relatively wide interval. At $C_A = 2$, $\hat{\omega}_- \approx -7.236$ and it agrees well with one of the dominant frequencies in Fig. 5 for $f_0 \approx f_0^{\text{th}}$. $\hat{\omega}_+ \approx -2.764$ approximates the upper band. This shows that the external force $f(t)$ also excites oscillations with frequencies $\hat{\omega}_{\pm}$. Resonances between Ω and $\hat{\omega}_-$ through the Kerr nonlinearity then create equidistant subharmonic frequencies in Fig. 5. This also indicates that the system can potentially be a frequency comb generator [37].

The distance between subharmonics increases due to increasing nonlinearity strength through f_0 , since the frequency $\hat{\omega}_-$ depends on the amplitude of the waves A_1 and B_1 when nonlinearities are taken into account.

Features of the spectra in Fig. 5 persist when the band is nearly flat, i.e., $C_A \approx 2$. In that case, the excited harmonic frequencies will mostly lie in band gaps that correspond to evanescent waves. These spatially localized modes are responsible for the dispersion suppression in the nonlinear lattice reported in Fig. 3, even though frequency of the injected plane wave is in the middle of a linear band. Supratransmission occurs when the modes become unstable.

Conclusion. We have shown properties of flat and nearly flat band lattices with an injected plane wave. Due to the interaction of their nearly flat band and nonlinearity, wave transmission can be suppressed even when its frequency is inside the band. However, in the defocusing nonlinearity, there is a threshold amplitude for a massive power surge in the transmission, i.e., supratransmission. We have shown that this is due to evanescent waves that become unstable. There is no supratransmission for the focusing nonlinearity because such spatially decaying states always exist and are stable.

We also studied the possibility to employ the system as a frequency comb generator due to nonlinear resonances between the injected wave and the natural edge mode of the system. The mode exists because of the topological nature of the lattice.

Our results are particularly relevant to waveguide arrays having the sawtooth configuration, where wave localization due to the presence of an accidental flat band was observed by fine tuning the intersite coupling coefficients [27]. Hence, power surge predicted here can in principle be detected in these systems. Nevertheless, the results will be of interest for researchers in other fields in physics where flat band systems may be realized.

Acknowledgments. This work was supported by a Faculty Start-Up Grant (Grant No. 8474000351/FSU-2021-011) by Khalifa University (KU). N.L. and I.K. also acknowledge support by KU through a Competitive Internal Research Awards Grant (Grant No. 8474000412/CIRA-2021-064). I.K. is also grateful for support from KU via Faculty Start-Up Grant No. 8474000352/FSU-2021-012.

-
- [1] B. Sutherland, Localization of electronic wave functions due to local topology, *Phys. Rev. B* **34**, 5208 (1986).
- [2] E. H. Lieb, Two theorems on the Hubbard model, *Phys. Rev. Lett.* **62**, 1201 (1989).
- [3] M. Arai, T. Tokihiro, T. Fujiwara, and M. Kohmoto, Strictly localized states on a two-dimensional Penrose lattice, *Phys. Rev. B* **38**, 1621 (1988).
- [4] L. Tang, D. Song, S. Xia, S. Xia, J. Ma, W. Yan, Y. Hu, J. Xu, D. Leykam, and Z. Chen, Photonic flat-band lattices and unconventional light localization, *Nanophotonics* **9**, 1161 (2020).
- [5] D. Leykam, A. Andreanov, and S. Flach, Artificial flat band systems: From lattice models to experiments, *Adv. Phys.: X* **3**, 1473052 (2018).
- [6] D. Leykam and S. Flach, Perspective: Photonic flatbands, *APL Photonics* **3**, 070901 (2018).
- [7] R. A. Vicencio Poblete, Photonic flat band dynamics, *Adv. Phys.: X* **6**, 1878057 (2021).
- [8] Z. Liu, E. J. Bergholtz, H. Fan, and A. M. Läuchli, Fractional Chern insulators in topological flat bands with higher Chern number, *Phys. Rev. Lett.* **109**, 186805 (2012).
- [9] E. Tang, J.-W. Mei, and X.-G. Wen, High-temperature fractional quantum Hall states, *Phys. Rev. Lett.* **106**, 236802 (2011).
- [10] D. López-González and M. I. Molina, Linear and nonlinear compact modes in quasi-one-dimensional flatband systems, *Phys. Rev. A* **93**, 043847 (2016).
- [11] W. Maimaiti, A. Andreanov, H. C. Park, O. Gendelman, and S. Flach, Compact localized states and flat-band generators in one dimension, *Phys. Rev. B* **95**, 115135 (2017).
- [12] N. Lazarides and G. P. Tsironis, Squid metamaterials on a Lieb lattice: From flat-band to nonlinear localization, *Phys. Rev. B* **96**, 054305 (2017).
- [13] N. Lazarides and G. P. Tsironis, Compact localized states in engineered flat-band \mathcal{PT} metamaterials, *Sci. Rep.* **9**, 4904 (2019).
- [14] Y. He, R. Mao, H. Cai, J.-X. Zhang, Y. Li, L. Yuan, S.-Y. Zhu, and D.-W. Wang, Flat-band localization in Creutz superradiance lattices, *Phys. Rev. Lett.* **126**, 103601 (2021).
- [15] R. A. Vicencio, C. Cantillano, L. Morales-Inostroza, B. Real, C. Mejía-Cortés, S. Weimann, A. Szameit, and M. I. Molina, Observation of localized states in Lieb photonic lattices, *Phys. Rev. Lett.* **114**, 245503 (2015).
- [16] S. Mukherjee, A. Spracklen, D. Choudhury, N. Goldman, P. Öhberg, E. Andersson, and R. R. Thomson, Observation of a localized flat-band state in a photonic Lieb lattice, *Phys. Rev. Lett.* **114**, 245504 (2015).
- [17] S. Mukherjee and R. R. Thomson, Observation of localized flat-band modes in a quasi-one-dimensional photonic rhombic lattice, *Opt. Lett.* **40**, 5443 (2015).
- [18] T. Biesenthal, M. Kremer, M. Heinrich, and A. Szameit, Experimental realization of \mathcal{PT} -symmetric flat bands, *Phys. Rev. Lett.* **123**, 183601 (2019).
- [19] M. Di Liberto, A. Hemmerich, and C. M. Smith, Topological Varma superfluid in optical lattices, *Phys. Rev. Lett.* **117**, 163001 (2016).
- [20] D. Taverner, N. G. R. Broderick, D. J. Richardson, R. I. Laming, and M. Ibsen, Nonlinear self-switching and multiple gap-soliton formation in a fiber Bragg grating, *Opt. Lett.* **23**, 328 (1998).
- [21] F. Geniet and J. Leon, Energy transmission in the forbidden band gap of a nonlinear chain, *Phys. Rev. Lett.* **89**, 134102 (2002).
- [22] R. Khomeriki, Nonlinear band gap transmission in optical waveguide arrays, *Phys. Rev. Lett.* **92**, 063905 (2004).
- [23] H. Susanto, Boundary driven waveguide arrays: Suprathreshold transmission and saddle-node bifurcation, *SIAM J. Appl. Math.* **69**, 111 (2008).
- [24] H. Susanto and N. Karjanto, Calculated threshold of supratransmission phenomena in waveguide arrays with saturable nonlinearity, *J. Nonlinear Opt. Phys. Mater.* **17**, 159 (2008).
- [25] K. Tse Ve Koon, P. Marquié, and P. Tchofo Dinda, Experimental observation of the generation of cutoff solitons in a discrete LC nonlinear electrical line, *Phys. Rev. E* **90**, 052901 (2014).
- [26] J.-W. Rhim and B.-J. Yang, Classification of flat bands according to the band-crossing singularity of Bloch wave functions, *Phys. Rev. B* **99**, 045107 (2019).
- [27] S. Weimann, L. Morales-Inostroza, B. Real, C. Cantillano, A. Szameit, and R. A. Vicencio, Transport in sawtooth photonic lattices, *Opt. Lett.* **41**, 2414 (2016).
- [28] K. Ji, X. Qi, S. Li, K. Han, Z. Wen, G. Zhang, and J. Bai, Nonlinearity-dependent asymmetric transmission in a sawtooth photonic lattice with defects, *Laser Phys.* **28**, 045404 (2018).
- [29] L. Du, Y. Zhang, and J.-H. Wu, Controllable unidirectional transport and light trapping using a one-dimensional lattice with non-Hermitian coupling, *Sci. Rep.* **10**, 1113 (2020).
- [30] B. Grémaud and G. G. Batrouni, Haldane phase on the sawtooth lattice: Edge states, entanglement spectrum, and the flat band, *Phys. Rev. B* **95**, 165131 (2017).
- [31] G. Orso and M. Singh, Pairs, trimers, and BCS-BEC crossover near a flat band: Sawtooth lattice, *Phys. Rev. B* **106**, 014504 (2022).
- [32] L. G. Phillips, G. De Chiara, P. Öhberg, and M. Valiente, Low-energy behavior of strongly interacting bosons on a flat-band lattice above the critical filling factor, *Phys. Rev. B* **91**, 054103 (2015).

- [33] P. Wang, L. Chen, C. Mi, Z. Meng, L. Huang, K. S. Nawaz, H. Cai, D.-W. Wang, S.-Y. Zhu, and J. Zhang, Synthesized magnetic field of a sawtooth superradiance lattice in Bose-Einstein condensates, *npj Quantum Inf.* **6**, 18 (2020).
- [34] T. Zhang and G.-B. Jo, One-dimensional sawtooth and zigzag lattices for ultracold atoms, *Sci. Rep.* **5**, 16044 (2015).
- [35] A. B. Togueu Motcheyo and J. E. Macías-Díaz, Nonlinear bandgap transmission with zero frequency in a cross-stitch lattice, *Chaos Solit. Fractals* **170**, 113349 (2023).
- [36] D. Sarafyan, Improved sixth-order Runge-Kutta formulas and approximate continuous solution of ordinary differential equations, *J. Math. Anal. Appl.* **40**, 436 (1972).
- [37] T. Fortier and E. Baumann, 20 years of developments in optical frequency comb technology and applications, *Commun. Phys.* **2**, 153 (2019).